CHEMISTRY OF MATERIALS

pubs.acs.org/cm

Article

Design Principle of Carbon-Supported Single-Atom Catalysts – Interplay between d-Orbital Periodicity and Local Hybridization

Zhengda He, Jingyang Wang,* and Bin Ouyang*

Cite This: https://doi.org/10.1021/acs.chemmater.3c02549

Read Online

ACCESS | Metrics & More | Article Recommendations | Supporting Information

ABSTRACT: Carbon-based single-atom catalysts (SACs) have been widely investigated as a potential alternative for noble-metal-based catalysts for the hydrogen evolution reaction (HER) and the oxygen reduction reaction (ORR). The rational design of such catalysts requires not only physical intuitions but also practical descriptors that can be directly applied in experiments. In this work, we establish a practical theoretical framework based on a comprehensive data set of SACs compromising 28 metals, 5 types of local environments, and adsorption calculations for 4 adsorbates (e.g., H/O/OH/OOH). We disentangle the complex trend of H/OH adsorption as an interplay between d-orbital periodicity and local hybridization, allowing for the estimation of the catalytic performance solely on the basis of the number of valence electrons. By utilizing this data set and theoretical framework, we have also identified several promising catalyst candidates and overlooked design strategies.

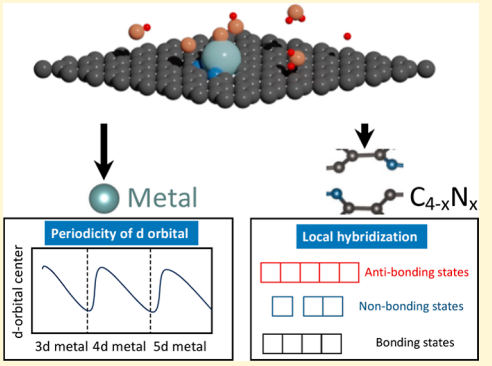

INTRODUCTION

The hydrogen evolution reaction (HER) and oxygen reduction reaction (ORR) are vital in many clean-energy technologies, e.g., fuel cells,[1] electrolyzers,[2] and metal−air batteries.[3−5] To date, the best catalysts for both reactions are noble metals,[6,7] which has driven us to work on reducing the content of noble metals in such catalysts while maintaining good catalytic performance. As part of such efforts, carbon-supported single-atom catalysts (SACs) have emerged as a potential solution. Particularly, it has been widely studied[8−11] that N-doped graphene sheets (denoted as M@$C_{4-x}N_x$) can serve as effective substrates for catalytically active metal sites. The utilization of M@$C_{4-x}N_x$ would potentially reduce the cost of catalysts as the main body is made from earth-abundant carbon. Additionally, it has been found that such catalysts do not require noble metals. For example, the Fe supported on N-doped graphene (usually denoted as Fe−N−C) catalyst shows high activity for ORR;[12,13] on the other hand, Co supported on N-doped graphene (Co−N−C) shows promising activity for HER.[14]

With emerging efforts for designing all kinds of M@$C_{4-x}N_x$, the design principles are not yet clear enough from a theoretical perspective. Proposing practical descriptors or predictors for SAC systems has attracted a lot of efforts, which can be largely categorized as either physics-based descriptors or machine-learning-based predictors. There have been multiple plausible works that proposed the local bond geometry,[13] d-band center,[13] center of a specific d-orbital,[15] magnetic moment,[13] and complex formula of coordination number and electronegativity[16] as physical descriptors. The descriptors that include the magnetic moment, local bond geometry, or quantities derived from electronic structure calculations (e.g., d-band center, band center of a specific d-orbital) have issues that those descriptors are challenging or impossible to be measured by experiments and thus are not very practical for guiding experiments. Xu et al. is the only work that has proposed a practical physical descriptor that predicts adsorption energy as a function of valence electrons, coordination amount, and electronegativity.[16] However, it has been indicated in a recent work that the proposed trend cannot be reproduced by other researchers.[17] On the other hand, the rapid development of machine learning has attracted various research works that utilize machine-learning models to predict adsorption energies.[17−21] It is without a doubt that machine learning can offer reasonable prediction accuracy for adsorption energies. However, such models provide limited physical explanation and sometimes suffer from the potential of overfitting small data set with a large number of hyperparameters.[22−24]

In this work, we present a complete data set for practical 3d, 4d, and 5d transition metals for M@$C_{4-x}N_x$ SACs to establish design principles that are both physical and easy to be used by experimentalists. Based on the computational data set consisting of 28 metals and 140 different catalysts (the

Received: October 6, 2023
Revised: January 15, 2024
Accepted: January 16, 2024

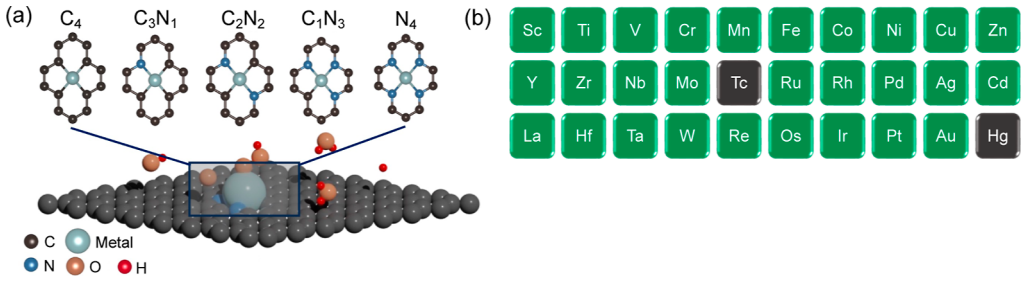

Figure 1. Structure of a slab model and metals selected in this study. (a) Schematic structure of the system investigated in this work. The upper figures represent five different local environments (denoted as C_4, C_3N_1, C_2N_2, C_1N_3, and N_4). The lower figure represents the slab model for SACs. The cyan, charcoal, blue, brown, and red spheres represent metal, C, N, O, and H atoms, respectively. (b) Cropped section of the periodic table illustrating the range of selected transition metals. Green blocks represent the transition metals (TM) investigated in this work. Black blocks represent TMs not investigated in this work.

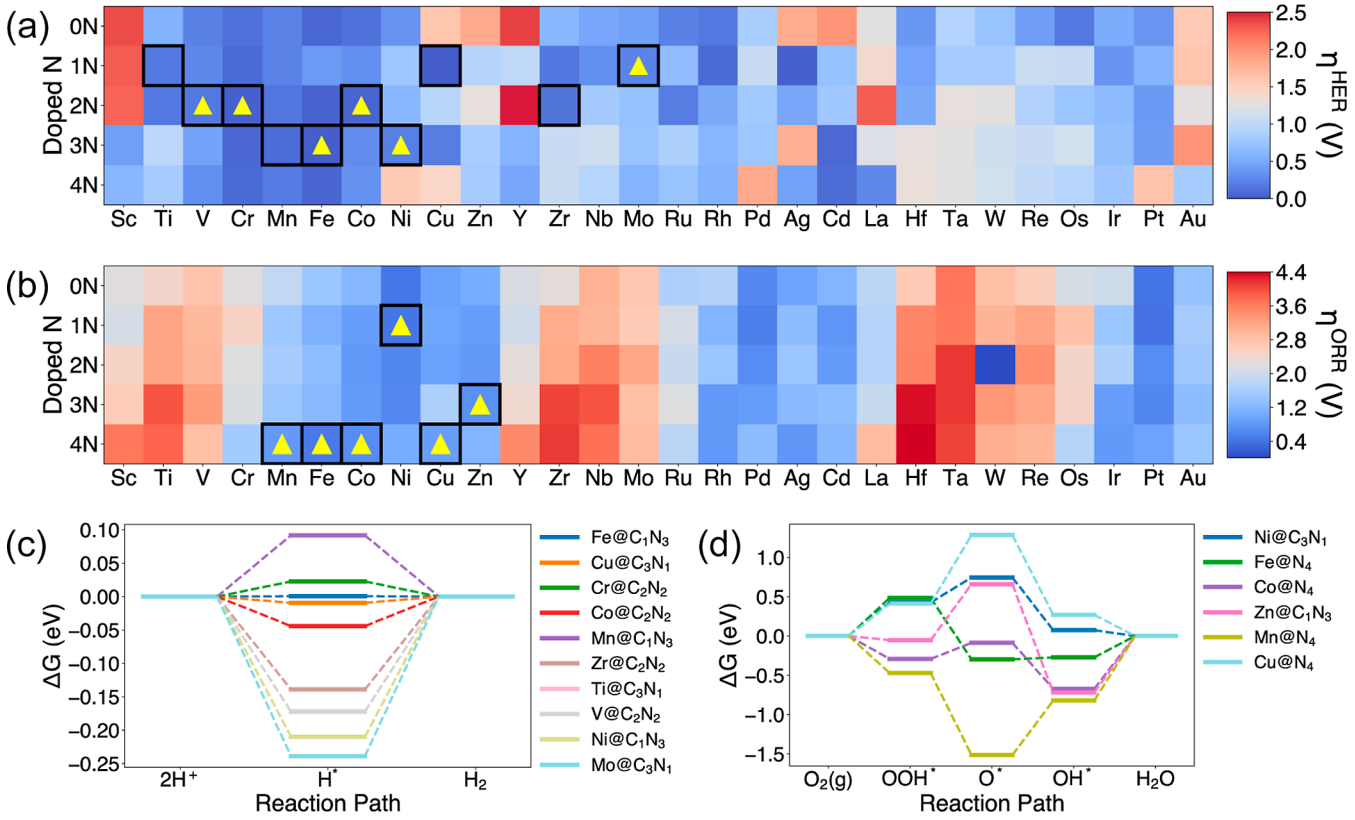

Figure 2. Heatmaps of overpotentials of HER and ORR and free-energy diagrams of promising catalysts. Heatmaps of thermodynamic overpotentials of (a) HER and (b) ORR for all investigated SACs. Red and blue represent high and low overpotentials, respectively. η^{HER} and η^{ORR} in the color bar represent the overpotential for HER and ORR, respectively. The $\eta_{W@C_2N_2}^{ORR}$ is excluded (represented by the dark-blue square) because the structure of OH adsorbed on W is not converged properly. The black squares in (a,b) represent the promising catalysts listed in (c,d), respectively. The yellow triangles show that the metals have been identified as potential catalysts for either HER or ORR in previous experimental works. Free-energy diagrams of (c) HER and (d) ORR at promising catalysts. The SACs are denoted as $M@C_{4-x}N_4$, where M is the metal and x = 0−4 represents the number of N atoms in the local environment.

structures of SACs and selected metals are shown in Figure 1), we have established the complex trend of H/OH adsorption as an interplay between the periodicity of d-orbitals and local hybridization. With the establishment of our theoretical framework, we can predict whether a given $M@C_{4-x}N_x$ can be a good catalyst with only knowledge of the metal species and the local $C_{4-x}N_x$ environment composition. Moreover, utilizing the established theoretical framework, we have identified several overlooked design handles for optimizing the HER/ORR performance of $M@C_{4-x}N_x$-based SACs.

METHODS

Slab Models. The atomic structure of the model system (as shown in Figure 1a) is established using an 8 × 8 supercell of a graphene sheet. A divacancy is created, followed by transition-metal doping. Given that each transition metal is 4-fold bonded with the graphene sheet, we enumerate all possible local environments by varying the composition of C and N atoms, denoted as $C_{4-x}N_x$ where x = 0−4, the number of N atoms. In addition, we highlight all selected transition metals in green, as illustrated in Figure 1b. The excluded metals are either a radioactive metal (Tc), a liquid metal (Hg), or rare-earth metals that are barely used for a graphene-based SAC.

https://doi.org/10.1021/acs.chemmater.3c02549
Chem. Mater. XXXX, XXX, XXX−XXX

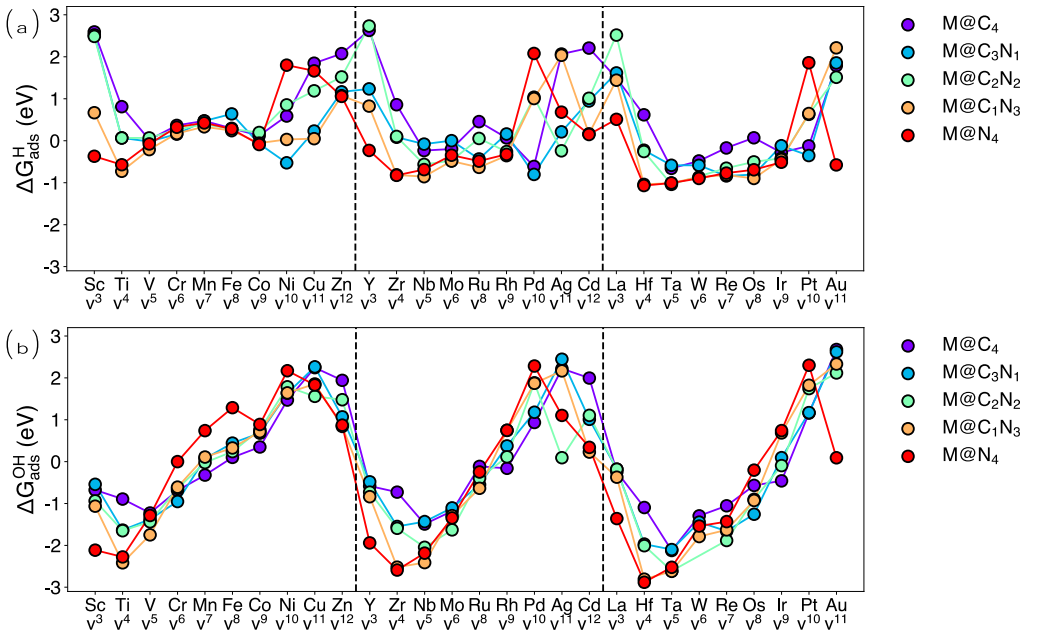

Figure 3. Trends of adsorption energies of H and OH. Adsorption energies of H and OH: (a) $\Delta G_{ads}{}^{H}$ and (b) $\Delta G_{ads}{}^{OH}$ on the investigated SACs are represented by circles. The color represents different local environments, as denoted in the legends. The solid lines which connect markers are guides for the eye. The vertical dashed lines separate 3d, 4d, and 5d transition metals. The number of valence electrons (shown as v^n) of elements is shown below the symbol of elements.

Density Functional Theory Calculations. All calculations in this study were performed with density functional theory (DFT) using the Vienna ab initio simulation (VASP) package.[25−27] The Perdew−Burke−Ernzerhof (PBE) functional was employed with spin polarization.[28] Core electrons were treated using the projector augmented wave method.[29,30] For the description of valence electrons, a plane-wave basis set with a kinetic energy cutoff of 520 eV was utilized. A reciprocal space discretization of 25 *K* points per $Å^{-1}$ was employed to sample the Brillouin zone. Geometry optimizations were executed until the force on each atom fell below 0.05 eV/Å, and the change in the total energy was less than 10^{-4} eV. The convergence criteria for self-consistent calculations were set as 10^{-4} eV. Gaussian smearing with a width of 0.05 eV was implemented to enhance the convergence of electronic minimization. The DFT-D2 method was utilized to incorporate van der Waals interaction into the computational model.[31] To investigate the overpotential of the HER (denoted as η^{HER}), one H was adsorbed on the metal for calculating the adsorption energy of H (denoted as $\Delta G_{ads}{}^{H}$). For ORR, intermediates O/OH/OOH were adsorbed on the metal for calculating $\Delta G_{ads}{}^{O/OH/OOH}$ and η^{ORR}. The details for calculating ΔG_{ads} and $\eta^{HER/ORR}$ are shown in Sections S1 and S2 in the Supporting Information.

RESULTS

Overpotentials and Free-Energy Diagrams of HER and ORR. The first two panels depicted in Figure 2 provide an overview of the computed overpotentials of the HER (Figure 2a) and ORR (Figure 2b), respectively. The most promising candidates decorated by non-noble metals are illustrated with black squares in Figure 2a,b. Several of these candidates are already reported experimentally (denoted by yellow triangles). Especially, V,[32] Cr,[32] Fe,[32] Co,[32] Ni,[33] and Mo[33] have been reported as catalytically active metal centers for HER and Mn,[34] Fe,[35] Co,[36] Ni,[37] Cu,[38,39] and Zn[40] as catalytically active metal sites for ORR. For HER, the materials are considered a promising candidates if $\eta_{HER} \leq 0.25$ V. For ORR, the selection criteria are $\eta_{ORR} \leq 0.39(\eta_{ORR}{}^{best}) + 0.5 = 0.89$ V, where 0.5 V is chosen arbitrarily since the definition of "good catalyst" cannot be explicitly defined. Our simulation results are comparable to previous computational (HER)[41] and experimental (ORR)[35] results (for detailed comparison, see Section S3 in Supporting Information). The free-energy profiles of promising catalysts for HER and ORR with non-noble metals are demonstrated in Figure 2c,d, respectively (full list of free-energy diagrams of HER and ORR on all investigated materials are provided in Figures S1 and S2, respectively). The promising catalysts are selected by picking up candidates with minimum overpotentials.

In Figure 2c, Fe with the local environment C_3N_1 (denoted as Fe@C_3N_1) turns out to be the best non-noble metal HER catalyst with the overpotential ($\eta^{HER}_{Fe@C_1NS}$ = 0.0006 V), followed by Cu@C_3N_1 ($\eta^{HER}_{Cu@CSN_1}$ = 0.00935 V), Cr@C_2N_2($\eta_{Cr@C_2N_2}$= 0.023 V), Co@C_2N_2 ($\eta^{HER}_{Co@C_2N_2}$ = 0.039 V), and Mn@C_1N_3 ($\eta^{HER}_{Mn@C_1NS}$ = 0.092 V). In contrast, the best noble-metal-decorated catalyst is Ag@C_3N_1, with $\eta^{HER}_{Ag@CSN_1}$ = 0.029 V. When it comes to ORR catalyst, as shown in Figure 2d, the best non-noble catalyst is Ni@C_3N_1 ($\eta^{ORR}_{Ni@CSN_1}$ = 0.42 V), which is just 0.03 V higher than the best catalyst with noble metals, e.g., Pt@C_3N_1 ($\eta^{ORR}_{Pt@CSN_1}$ = 0.39 V), followed by Pt@C_4 ($\eta^{ORR}_{Pt@C_4}$ = 0.40 V). Other promising candidates are Fe@N_4 ($\eta^{ORR}_{Fe@N_4}$ = 0.49 V), Co@N_4 ($\eta^{ORR}_{Co@N_4}$ = 0.67 V), Zn@C_1N_3 ($\eta^{ORR}_{Zn@C_1NS}$ = 0.72 V), Mn@N_4 ($\eta^{ORR}_{Mn@N_4}$ = 0.87 V), and Cu@N_4 ($\eta^{ORR}_{Cu@N_4}$ = 0.87 V). The free-energy diagrams of ORR for promising catalysts under different applied potentials are shown in Figure S3.

Adsorption Energies of H and OH. To elucidate more details about the origin of overpotential, we plotted the adsorption energy on the most critical adsorption step, e.g., the adsorption of H for the HER (Figure 3a) and the adsorption of OH for the ORR (Figure 3b). These two steps are critical because ΔG^{H}_{ads} and ΔG^{OH}_{ads} are widely used as descriptors to

https://doi.org/10.1021/acs.chemmater.3c02549
Chem. Mater. XXXX, XXX, XXX−XXX

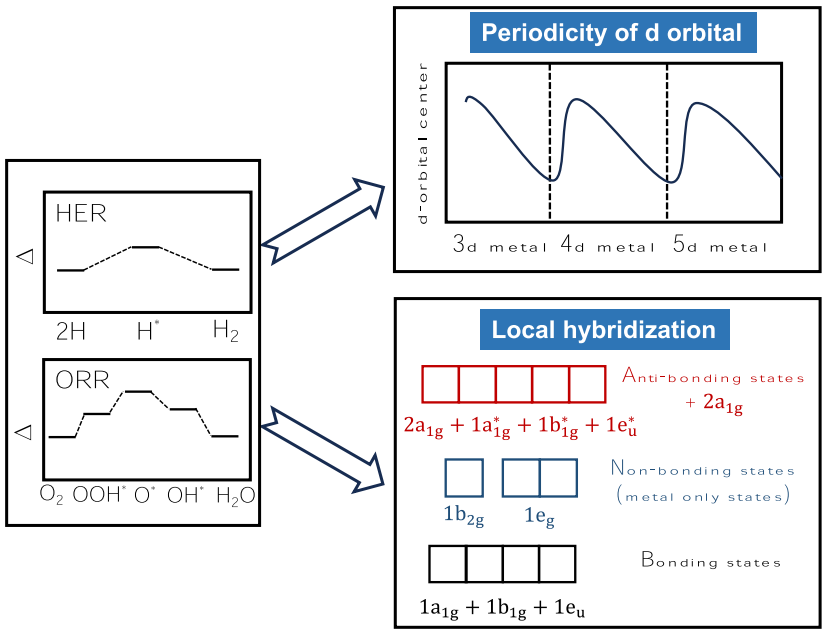

Figure 4. Schematic of the governing factors for $\Delta G_{ads}^{H/OH}$. Two factors are proposed: (1) periodicity of the d-orbital center (illustrated in the upper right panel) and (2) local hybridization between the metal and the local environment (illustrated in the lower right panel).

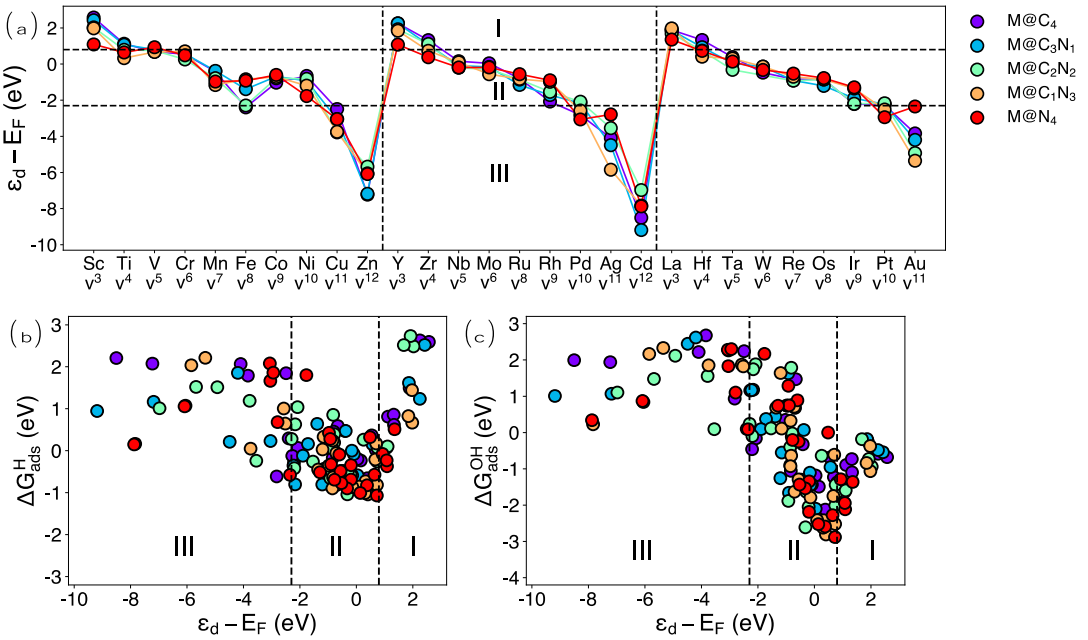

Figure 5. Trend of the d-orbital center and correlation between the d-orbital center and adsorption energies of H/OH. (a) d-Orbital center with respect to the Fermi level ($\varepsilon_d - E_F$), represented by circles. Different colors of markers represent different local environments which are denoted in the legend. The circles are connected by solid lines as guide to the eyes. The two vertical dashed lines separate 3d, 4d, and 5d metals. The two horizontal dashed lines separate metals into three groups based on $\varepsilon_d - E_F$ with different background colors, labeled by the text in each part (e.g., I, II, and III). The number of valence electrons (denoted as v^n) of metals is shown in the second line of *x*-axis labels. Correlations between ΔG_{ads}^{H}, ΔG_{ads}^{OH}, and $\varepsilon_d - E_F$ are shown in subfigures (b,c). Same markers as (a) were used. The vertical lines separate metals into three groups with distinct background colors and labels, similar to (a).

evaluate the activity of catalysts of HER[42] and ORR,[6] respectively. We plot the energies of ΔG_{ads}^{H} and ΔG_{ads}^{OH} on the same energy scale for easy comparison. The trends of ΔG_{ads}^{O} and ΔG_{ads}^{OOH} are shown in Figures S3 and S4 in Supporting Information, respectively.

We can observe four interesting trends in Figure 3a: (1) there is a lack of clear pattern for $\Delta G_{ads}{}^{H}$ values (shown in Figure 3a), which is consistent with the η^{HER} (as shown in Figure 2a); (2) in contrast to H adsorption, there is a pronounced periodic pattern for $\Delta G_{ads}{}^{OH}$. Specifically, $\Delta G_{ads}{}^{OH}$ decreases from v^3 (metal with 3 valence electrons) to v^4 metals, then increases from v^5 to v^{12} metals. The valence electrons for all metals are shown as x labels in Figure 3a,b. (3) For v^{3-4} metals and v^{10-12} metals, $\Delta G_{ads}{}^{H}$ is highly sensitive to local coordination. In some cases (e.g., Ni and Cu), the largest deviation can be as high as 3 eV. In contrast, $\Delta G_{ads}{}^{OH}$ have

https://doi.org/10.1021/acs.chemmater.3c02549
Chem. Mater. XXXX, XXX, XXX−XXX

much smaller variation, typically less than 1 eV, depending on the local coordination. (4) For v^{5-9} metals, the $\Delta G_{ads}{}^{H}$ values are nearly identical across all local environments for 3d metals and very similar for 4d and 5d metals. All of these observations reveal that the H adsorption process can be fundamentally different from OH adsorption.

DISCUSSION

Two Deterministic Factors for $\Delta G_{ads}{}^{H/OH}$. To provide insights into the distinct behaviors of H and OH adsorption, we propose to attribute the origin to two factors: the periodicity of the d orbital and the diverse hybridization mechanism of metal−C−N complexes and their interactions with H or OH molecules. The schematic of our proposed theoretical framework is depicted in Figure 4. More specifically, the periodicity of the d-orbital establishes the baseline of the d-orbital center, which in turn determines the approximate position of $\Delta G_{ads}^{H/OH}$. On the other hand, the local hybridization between metal and C/N, as well as metal−C−N with H or OH, acts as a secondary effect that further refines the exact value of $\Delta G_{ads}^{H/OH}$. In the following two sections, we elaborate on the impact of d-orbital periodicity and local hybridization individually, subsequently addressing the origins of the four aforementioned observations.

Periodicity of d-Orbitals. The periodicity of d-orbitals can be clearly demonstrated by Figure 5a. Furthermore, the d-orbital center with respect to the Fermi level ($\varepsilon_d - E_F$, where E_F is the Fermi level) of metal is much more related to the number of d electrons rather than the local environment. We then directly plot the $\Delta G_{ads}{}^{H/OH}$ values as a function of $\varepsilon_d - E_F$ in Figure 5b,c, respectively.

It can be inferred from Figure 5b,c that there is a complex correlation between $\Delta G_{ads}^{H/OH}$ and $\varepsilon_d - E_F$. To help disentangle these correlations, the data points in both Figure 5b,c are divided into three different groups depending on the sign of correlation between $\varepsilon_d - E_F$ and $\Delta G_{ads}{}^{H/OH}$. Similar correlations for $\Delta G_{ads}{}^{O/OOH}$ are shown in Figure S5 in Supporting Information. These groups are also reflected in Figure 5a using different color shading, which also reveals that the metals in these groups in general have v^3−v^4 (group I, shaded blue), v^5−v^9 (group II, shaded green), and v^{10}−v^{12} (group III, shaded yellow) electronic configurations. With such division of data, we can see an approximately linear correlation between $\Delta G_{ads}{}^{H/OH}$ and $\varepsilon_d - E_F$ at each group, which supports the general idea of d-orbital center.[43,44] However, the fact that the sign of correlation depends on the electronic structure of d orbitals also reveals that there is an additional mechanism on top of the d orbital periodicity.

Diverse Mechanism of Hybridization. For understanding the relation between the local environment and adsorption energies, we proposed a model to understand the secondary factor that governs $\Delta G_{ads}^{H/OH}$ through molecular orbital theory. Our model is inspired by the frontier orbital concept formulated by Hoffman and co-workers.[45] There are two types of hybridizations in the investigated system, e.g., (1) hybridization between d-orbitals in the metal site and molecular orbitals of the local environment in the substrate and (2) hybridization between the frontier orbital in OH/H and the catalyst. Both hybridizations are critical in determining the adsorption energy as the first hybridization sets up the energy levels of the catalyst, while the second hybridization is the actual origin of different adsorption energies. The schematic of the model is shown in Figure 6. The hybridized

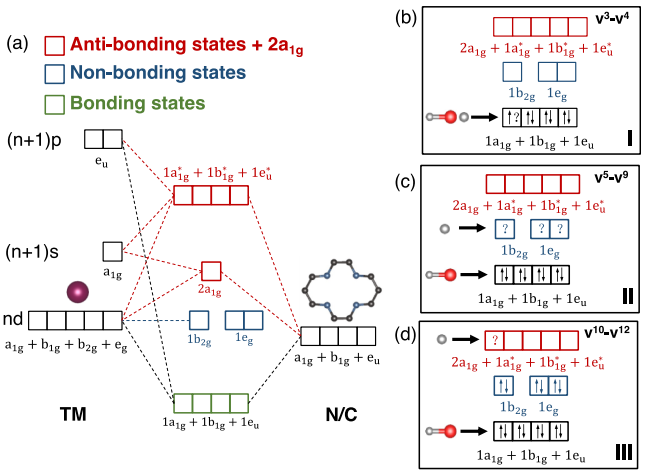

Figure 6. Molecular orbital model for understanding the adsorption of H/OH on SACs. (a) Molecular orbital diagram of the $M@C_{4-x}N_x$ system. Metal site, depicted as a purple sphere, is denoted as TM. The local environment is $C_{4-x}N_x$, where C in graphene and coordinated C/N are represented by charcoal spheres and dark-blue spheres, respectively. The green, blue, and red boxes represent the bonding, nonbonding, and antibonding states $+2a_{1g}$, respectively. The labels below boxes represent the names of the orbitals. Occupation of states after adsorption of OH on (b) group I metals (with v^3−v^4 electronic states), (c) group II metals (with v^5−v^9 electronic states), and (d) group III metals (with v^{10}−v^{12} electronic states). Up and down arrows represent electrons with spin up and down, respectively. The question mark represents the possible state for the electron from adsorbates (H/OH) to occupy. The red and gray spheres represent the O and H atoms, respectively.

molecular orbitals between the metal site (M) and the local environment ($C_{4-x}N_x$, where $x = 0$−4) is shown in Figure 6a. For clarity, we merge different molecular orbitals into three groups denoted by different colors. More specifically, green color indicates bonding orbitals, blue color indicates nonbonding orbitals, and red color indicates the a_{1g} state above nonbonding states and all antibonding states. It is worth noting that the merge of different molecular orbitals does not indicate degeneracy but rather our way of classifying interacting orbitals with adsorbates (H or OH) that will facilitate our analysis.

With the establishment of molecular orbitals, as shown in Figure 6a, we can then explain the diverse dependency of local coordination of adsorption energy, as shown in Figure 3. Depending on the filling of molecular orbitals, H and OH will interact differently with the adsorbent. The metals can be categorized into three groups: v^3−v^4 metals (group I), v^5−v^9 (group II), and v^{10}−v^{12} (group III).

Regarding the adsorption of OH, the energy level of the O state is comparable to that of C or N in terms of electronegativity. As a result, the O state rehybridizes with the bonding states of $M@C_{4-x}N_x$ as shown in Figure 6b−d. Due to rehybridization with C and N states, ΔG_{ads}^{OH} will be sensitive to the local environment (e.g., C and N states) for all groups of metals. For adsorption of H, the energy level of 1s H is much higher than that of O, and the state of H will tend to interact with the highest unoccupied state in $M@C_{4-x}N_x$ like a ligand group. For group I metals, the bonding state is not fully occupied. In this case, H interacts with the bonding state, as shown in Figure 6b. Such states are formed from the hybridization between metal states and the local environment (e.g., C and N states), leading to sensitive ΔG_{ads}^{H} values to the

https://doi.org/10.1021/acs.chemmater.3c02549
Chem. Mater. XXXX, XXX, XXX−XXX

local environment. Conversely, for group II metals (as shown in Figure 6c), H interacts with the nonbonding states contributed solely by the metal d states, making ΔG^{H}_{ads} insensitive to the local environment (e.g., C and N states). For group III metals (as shown in Figure 6d), since the nonbonding states of metal are fully occupied, H interacts with antibonding or $2a_{1g}$ states, and both states consist of contribution from the local environment (e.g., C, N states), making ΔG^{H}_{ads} also sensitive to the local environment.

In conclusion, the theoretical framework in Figure 6 can provide a full understanding of the trends of adsorption energies shown in Figure 3 and in the section "Adsorption Energies of H and OH". More specifically, H adsorption in $M@C_{4-x}N_x$ is more sensitive to the local environment when M is an early (v^{3-4}) or late (v^{10-12}) transition metal but will be insensitive to the middle group of metals (v^{5-9}). This reveals the fact that local structure engineering through N doping is not very effective for v^{5-9} metals. This will be an important discovery, considering that we found many promising candidates for HER with a v^{5-9} electronic configuration, as shown in Figures 2 and 3. For early and late transition metals, the sensitive adsorption energy on the local environment also opens the gate for tuning catalytic activity through different functionalization methods, not only by changing doped metals but also by introducing defect−defect interactions and the coordination environment of metal.

On the other hand, OH adsorption is in principle dominated by the d-orbital center and further fine-tuned with the hybridization between $M@C_{4-x}N_x$ and the OH group. The ΔG^{OH}_{ads} generally follows the periodicity of the d-orbital center (shown in Figure 3b) and has relatively less tunable space compared with some cases in ΔG^{H}_{ads}. This reveals that the role of some critical metals is not so easy to replace, and to name a few, Mn, Fe, Co, and Ni are computed to have superior ΔG^{OH}_{ads}, largely due to their unique electronegativity. This adds some constraints in the actual design of $M@C_{4-x}N_x$ catalysts for ORR applications.

In addition to the proposed physical understanding, we also want to point out that there could be limitations in the presented analysis. Specifically, (1) the DFT calculations can be easily trapped into a local minimum. As being pointed out by Di Liberto et al., incorrected conducted DFT calculations can sometimes lead to wrong understanding of design principles.[17] We carefully checked our DFT relaxation, including starting the calculations with different geometry perturbations. To promote the communication and understanding of such system, the raw data from DFT is also open-sourced.[46] (2) Whether or not performing calculation using DFT + U is an unsolved problem for $M@C_{4-x}N_x$. One of the most widely used *U* values for transition metals are benchmarked from the formation energy of metal oxides, which apparently does not apply in the application of carbon-supported catalysts.[47] In several existing $M@C_{4-x}N_x$ literature, people used different sets of *U* values, where a detailed justification of the selection of *U* values is absent.[13,16,17,48−50] We decided to avoid *U* in this work. But it is possible that the addition of U values will significantly change the trend of adsorption energy. While it has been demonstrated that hybrid functionals can enhance calculation accuracy,[48,51] the PBE functional, which is utilized in this study, should have less concern in terms of capturing the general trends.[20,21,52,53] (3) The stability of our predicted materials in a realistic catalytic environment (e.g., aqueous solution) is another crucial factor to consider. To provide a straightforward assessment of the stability of all catalysts investigated, the binding energy of transition metals on N-doped graphene substrates with different C/N ratios in a coordinated environment is presented in Figure S6 in Supporting Information. Since HER/ORR mostly happen in aqueous solution, the solvation effect could also influence the activity trend. Such DFT results can be a useful starting point for assessing more complex interactions under solution conditions.

CONCLUSIONS

To summarize our study, with high-throughput DFT calculations, we have delivered a complete data set of N-doped carbon-supported SACs ($M@C_{4-x}N_x$) and identified promising material candidates for both the HER and ORR. Our findings deconvolute the critical factors that govern adsorption energies of H/OH into the periodicity of the d-orbital center and local hybridization. With the proposed framework from molecular orbital theory, the diverse behavior of H and OH adsorption during HER and ORR reactions can be well explained. The theoretical paradigm proposed also underscores several overlooked design strategies for making good SACs.

ASSOCIATED CONTENT

Data Availability Statement

The input (INCAR, KPOINTS, and POTCAR labels) and output files (CONTCAR and OSZICAR) for VASP calculations, and free-energy diagrams for HER and ORR on all substrates can be found at https://jeff-oakley.github.io/SAC_HOER_data/. All the data not included here are available from the corresponding authors upon reasonable request.

Supporting Information

The Supporting Information is available free of charge at https://pubs.acs.org/doi/10.1021/acs.chemmater.3c02549.

Additional computational details for calculating the overpotential and adsorption energies; overpotential compared with previous works; free-energy diagrams of HER/ORR for all materials; adsorption energies of O and OOH; correlation between the d-band center and the adsorption energies of O/OOH; binding energies of transition-metal atoms; magnetic moment of transition-metal atoms; structures of adsorbates for the promising catalysts of HER and ORR (PDF)

AUTHOR INFORMATION

Corresponding Authors

Jingyang Wang − *Department of Materials Science and Engineering, University of California, Berkeley, California 94720, United States; School of Sustainable Energy and Resources, Nanjing University, Suzhou 215163, P. R. China;* orcid.org/0000-0002-0174-9334; Email: jingyang_wang@berkeley.edu

Bin Ouyang − *Department of Chemistry and Biochemistry, Florida State University, Tallahassee, Florida 32304, United States;* orcid.org/0000-0002-8181-6815; Email: bouyang@fsu.edu

https://doi.org/10.1021/acs.chemmater.3c02549
Chem. Mater. XXXX, XXX, XXX−XXX

Author

Zhengda He − *Department of Chemistry and Biochemistry, Florida State University, Tallahassee, Florida 32304, United States*

Complete contact information is available at: https://pubs.acs.org/10.1021/acs.chemmater.3c02549

Author Contributions

Z.H., J.W., and B.O. performed the ab initio simulations. Z.H. and B.O. conducted the theoretical analysis of the data. B.O. supervised the project, provided critical feedback, and helped guide the research. All authors discussed the results, contributed to the final manuscript, and gave final approval for publication.

Notes

The authors declare no competing financial interest.

■ ACKNOWLEDGMENTS

We acknowledge support from the startup funding from Florida State University. The Computational resources are provided by the Advanced Cyberinfrastructure Coordination Ecosystem: Services & Support (ACCESS), the National Energy Research Scientific Computing Center (NERSC), a DOE Office of Science User Facility supported by the Office of Science and the U.S. Department of Energy under contract no. DE-AC02-05CH11231, and Research Computing Center (RCC) at Florida State University. The computation and data processing are also supported by the supercomputing resources from the Department of Energy's Office of Energy Efficiency and Renewable Energy at the National Renewable Energy Laboratory.

■ REFERENCES

(1) Markovic, N.; Ross, P. N. Surface science studies of model fuel cell electrocatalysts. *Surf. Sci. Rep.* **2002**, *45* (4−6), 117−229.

(2) Walter, M. G.; Warren, E. L.; McKone, J. R.; Boettcher, S. W.; Mi, Q.; Santori, E. A.; Lewis, N. S. Solar Water Splitting Cells. *Chem. Rev.* **2010**, *110* (11), 6446−6473.

(3) Lu, J.; Li, L.; Park, J.-B.; Sun, Y.-K.; Wu, F.; Amine, K. Aprotic and Aqueous Li-O2 Batteries. *Chem. Rev.* **2014**, *114* (11), 5611−5640.

(4) Peng, Z.; Freunberger, S. A.; Chen, Y.; Bruce, P. G. A Reversible and Higher-Rate Li-O2 Battery. *Science* **2012**, *337* (6094), 563−566.

(5) Yan, S.; Feng, Y.; Lin, J.; Wang, Y. Metal-Redox Bicatalysis Batteries for Energy Storage and Chemical Production. *Adv. Mater.* **2023**, *35*, 2212078.

(6) Kulkarni, A.; Siahrostami, S.; Patel, A.; Nørskov, J. K. Understanding catalytic activity trends in the oxygen reduction reaction. *Chem. Rev.* **2018**, *118* (5), 2302−2312.

(7) Dubouis, N.; Grimaud, A. The hydrogen evolution reaction: from material to interfacial descriptors. *Chem. Sci.* **2019**, *10* (40), 9165−9181.

(8) Zhuo, H.-Y.; Zhang, X.; Liang, J.-X.; Yu, Q.; Xiao, H.; Li, J. Theoretical Understandings of Graphene-based Metal Single-Atom Catalysts: Stability and Catalytic Performance. *Chem. Rev.* **2020**, *120* (21), 12315−12341.

(9) Zhang, Q.; Zhang, X.; Wang, J.; Wang, C. Graphene-supported single-atom catalysts and applications in electrocatalysis. *Nanotechnology* **2021**, *32* (3), 032001.

(10) Yam, K. M.; Guo, N.; Jiang, Z.; Li, S.; Zhang, C. Graphene-Based Heterogeneous Catalysis: Role of Graphene. *Catalysts* **2020**, *10* (1), 53.

(11) Dai, Y.; Kong, F.; Tai, X.; Zhang, Y.; Liu, B.; Cai, J.; Gong, X.; Xia, Y.; Guo, P.; Liu, B.; et al. Advances in Graphene-Supported Single-Atom Catalysts for Clean Energy Conversion. *Electrochem. Energy Rev.* **2022**, *5* (S2), 22.

(12) Shen, H.; Thomas, T.; Rasaki, S. A.; Saad, A.; Hu, C.; Wang, J.; Yang, M. Oxygen Reduction Reactions of Fe-N-C Catalysts: Current Status and the Way Forward. *Electrochem. Energy Rev.* **2019**, *2* (2), 252−276.

(13) Liu, K.; Fu, J.; Lin, Y.; Luo, T.; Ni, G.; Li, H.; Lin, Z.; Liu, M. Insights into the activity of single-atom Fe-N-C catalysts for oxygen reduction reaction. *Nat. Commun.* **2022**, *13* (1), 2075.

(14) Huang, K.; Wei, Z.; Liu, J.; Gong, Z.; Liu, J.; Yan, M.; He, G.; Gong, H.; Hu, Y.; He, Y.; et al. Engineering the Morphology and Microenvironment of a Graphene-Supported Co-N-C Single-Atom Electrocatalyst for Enhanced Hydrogen Evolution. *Small* **2022**, *18* (19), 2201139.

(15) Wang, Y.; Liang, Y.; Bo, T.; Meng, S.; Liu, M. Orbital dependence in single-atom electrocatalytic reactions. *J. Phys. Chem. Lett.* **2022**, *13* (25), 5969−5976.

(16) Xu, H.; Cheng, D.; Cao, D.; Zeng, X. C. A universal principle for a rational design of single-atom electrocatalysts. *Nat. Catal.* **2018**, *1* (5), 339−348.

(17) Di Liberto, G.; Cipriano, L. A.; Pacchioni, G. Universal principles for the rational design of single atom electrocatalysts? handle with care. *ACS Catal.* **2022**, *12* (10), 5846−5856.

(18) Schlexer Lamoureux, P.; Winther, K. T.; Garrido Torres, J. A.; Streibel, V.; Zhao, M.; Bajdich, M.; Abild-Pedersen, F.; Bligaard, T. Machine Learning for Computational Heterogeneous Catalysis. *ChemCatChem* **2019**, *11* (16), 3581−3601.

(19) Mou, L.-H.; Han, T.; Smith, P. E. S.; Sharman, E.; Jiang, J. Machine Learning Descriptors for Data-Driven Catalysis Study. *Advanced Science* **2023**, *10*, 2301020.

(20) Fung, V.; Hu, G.; Wu, Z.; Jiang, D.-e. Descriptors for hydrogen evolution on single atom catalysts in nitrogen-doped graphene. *J. Phys. Chem. C* **2020**, *124* (36), 19571−19578.

(21) Tamtaji, M.; Chen, S.; Hu, Z.; Goddard Iii, W. A.; Chen, G. A Surrogate Machine Learning Model for the Design of Single-Atom Catalyst on Carbon and Porphyrin Supports towards Electrochemistry. *J. Phys. Chem. C* **2023**, *127* (21), 9992−10000.

(22) Le, T.; Epa, V. C.; Burden, F. R.; Winkler, D. A. Quantitative Structure-Property Relationship Modeling of Diverse Materials Properties. *Chem. Rev.* **2012**, *112* (5), 2889−2919.

(23) Toyao, T.; Maeno, Z.; Takakusagi, S.; Kamachi, T.; Takigawa, I.; Shimizu, K.-i. Machine Learning for Catalysis Informatics: Recent Applications and Prospects. *ACS Catal.* **2020**, *10* (3), 2260−2297.

(24) Lewis-Atwell, T.; Townsend, P. A.; Grayson, M. N. Machine learning activation energies of chemical reactions. *Wiley Interdiscip. Rev. Comput. Mol. Sci.* **2022**, *12* (4), No. e1593.

(25) Kresse, G.; Hafner, J. Ab initio molecular dynamics for liquid metals. *Phys. Rev. B* **1993**, *47* (1), 558−561.

(26) Kresse, G.; Hafner, J. Ab initio molecular-dynamics simulation of the liquid-metal-amorphous-semiconductor transition in germanium. *Phys. Rev. B* **1994**, *49* (20), 14251−14269.

(27) Kresse, G.; Furthmüller, J. Efficiency of ab-initio total energy calculations for metals and semiconductors using a plane-wave basis set. *Comput. Mater. Sci.* **1996**, *6* (1), 15−50.

(28) Perdew, J. P.; Burke, K.; Ernzerhof, M. Generalized gradient approximation made simple. *Phys. Rev. Lett.* **1996**, *77* (18), 3865−3868.

(29) Blöchl, P. E. Projector augmented-wave method. *Phys. Rev. B* **1994**, *50* (24), 17953−17979.

(30) Kresse, G.; Joubert, D. From ultrasoft pseudopotentials to the projector augmented-wave method. *Phys. Rev. B* **1999**, *59* (3), 1758−1775.

(31) Grimme, S. Semiempirical GGA-type density functional constructed with a long-range dispersion correction. *J. Comput. Chem.* **2006**, *27* (15), 1787−1799.

(32) Hossain, M. D.; Liu, Z.; Zhuang, M.; Yan, X.; Xu, G. L.; Gadre, C. A.; Tyagi, A.; Abidi, I. H.; Sun, C. J.; Wong, H.; et al. Rational design of graphene-supported single atom catalysts for hydrogen evolution reaction. *Adv. Energy Mater.* **2019**, *9* (10), 1803689.

(33) Fan, L.; Liu, P. F.; Yan, X.; Gu, L.; Yang, Z. Z.; Yang, H. G.; Qiu, S.; Yao, X. Atomically isolated nickel species anchored on graphitized carbon for efficient hydrogen evolution electrocatalysis. *Nat. Commun.* **2016**, *7* (1), 10667.
(34) Li, J.; Chen, M.; Cullen, D. A.; Hwang, S.; Wang, M.; Li, B.; Liu, K.; Karakalos, S.; Lucero, M.; Zhang, H.; et al. Atomically dispersed manganese catalysts for oxygen reduction in proton-exchange membrane fuel cells. *Nat. Catal.* **2018**, *1* (12), 935−945.
(35) Liu, L.; Liu, S.; Li, L.; Qi, H.; Yang, H.; Huang, Y.; Wei, Z.; Li, L.; Xu, J.; Liu, B. A general method to construct single-atom catalysts supported on N-doped graphene for energy applications. *J. Mater. Chem. A* **2020**, *8* (13), 6190−6195.
(36) Shi, C.; Liu, Y.; Qi, R.; Li, J.; Zhu, J.; Yu, R.; Li, S.; Hong, X.; Wu, J.; Xi, S.; et al. Hierarchical N-doped carbon spheres anchored with cobalt nanocrystals and single atoms for oxygen reduction reaction. *Nano Energy* **2021**, *87*, 106153.
(37) Jiang, H.; Xia, J.; Jiao, L.; Meng, X.; Wang, P.; Lee, C.-S.; Zhang, W. Ni single atoms anchored on N-doped carbon nanosheets as bifunctional electrocatalysts for Urea-assisted rechargeable Zn-air batteries. *Appl. Catal., B* **2022**, *310*, 121352.
(38) Shang, H.; Zhou, X.; Dong, J.; Li, A.; Zhao, X.; Liu, Q.; Lin, Y.; Pei, J.; Li, Z.; Jiang, Z.; et al. Engineering unsymmetrically coordinated Cu-S1N3 single atom sites with enhanced oxygen reduction activity. *Nat. Commun.* **2020**, *11* (1), 3049.
(39) Yang, L.; Xu, H.; Liu, H.; Zeng, X.; Cheng, D.; Huang, Y.; Zheng, L.; Cao, R.; Cao, D. Oxygen-Reconstituted Active Species of Single-Atom Cu Catalysts for Oxygen Reduction Reaction. *Research* **2020**, *2020*, 7593023.
(40) Li, J.; Chen, S.; Yang, N.; Deng, M.; Ibraheem, S.; Deng, J.; Li, J.; Li, L.; Wei, Z. Ultrahigh-Loading Zinc Single-Atom Catalyst for Highly Efficient Oxygen Reduction in Both Acidic and Alkaline Media. *Angew. Chem., Int. Ed.* **2019**, *58* (21), 7035−7039.
(41) Hossain, M. D.; Liu, Z.; Zhuang, M.; Yan, X.; Xu, G.-L.; Gadre, C. A.; Tyagi, A.; Abidi, I. H.; Sun, C.-J.; Wong, H.; et al. Rational Design of Graphene-Supported Single Atom Catalysts for Hydrogen Evolution Reaction. *Adv. Energy Mater.* **2019**, *9* (10), 1803689.
(42) Nørskov, J. K.; Bligaard, T.; Logadottir, A.; Kitchin, J.; Chen, J. G.; Pandelov, S.; Stimming, U. Trends in the exchange current for hydrogen evolution. *J. Electrochem. Soc.* **2005**, *152* (3), J23.
(43) Hammer, B.; Nørskov, J. Electronic factors determining the reactivity of metal surfaces. *Surf. Sci.* **1995**, *343* (3), 211−220.
(44) Hammer, B.; Norskov, J. K. Why gold is the noblest of all the metals. *Nature* **1995**, *376* (6537), 238−240.
(45) Hoffmann, R. *Solids and Surfaces: A Chemist's View of Bonding in Extended Structures*; John Wiley & Sons, 1991.
(46) https://github.com/Jeff-oakley/SAC_HOER_data (accessed from 01/11/2024).
(47) Jain, A.; Hautier, G.; Ong, S. P.; Moore, C. J.; Fischer, C. C.; Persson, K. A.; Ceder, G. Formation enthalpies by mixing GGA and GGA+ U calculations. *Phys. Rev. B* **2011**, *84* (4), 045115.
(48) Barlocco, I.; Cipriano, L. A.; Di Liberto, G.; Pacchioni, G. Modeling Hydrogen and Oxygen Evolution Reactions on Single Atom Catalysts with Density Functional Theory: Role of the Functional. *Adv. Theory Simul.* **2022**, *6*, 2200513.
(49) Gong, L.; Zhang, D.; Lin, C.-Y.; Zhu, Y.; Shen, Y.; Zhang, J.; Han, X.; Zhang, L.; Xia, Z. Catalytic Mechanisms and Design Principles for Single-Atom Catalysts in Highly Efficient CO2 Conversion. *Adv. Energy Mater.* **2019**, *9* (44), 1902625.
(50) Cipriano, L. A.; Di Liberto, G.; Pacchioni, G. Superoxo and Peroxo Complexes on Single-Atom Catalysts: Impact on the Oxygen Evolution Reaction. *ACS Catal.* **2022**, *12* (19), 11682−11691.
(51) Patel, A. M.; Ringe, S.; Siahrostami, S.; Bajdich, M.; Nørskov, J. K.; Kulkarni, A. R. Theoretical Approaches to Describing the Oxygen Reduction Reaction Activity of Single-Atom Catalysts. *J. Phys. Chem. C* **2018**, *122* (51), 29307−29318.
(52) Zhang, N. N.; Li, J.; Xiao, H. The Key Role of Competition between Orbital and Electrostatic Interactions in the Adsorption on Transition Metal Single-Atom Catalysts Anchored by N-doped Graphene. *ChemCatChem* **2022**, *14* (16), No. e202200275.
(53) Di Liberto, G.; Cipriano, L. A.; Pacchioni, G. Single Atom Catalysts: What Matters Most, the Active Site or The Surrounding? *ChemCatChem* **2022**, *14* (19), No. e202200611.

https://doi.org/10.1021/acs.chemmater.3c02549
Chem. Mater. XXXX, XXX, XXX−XXX